Journal of Catalysis 284 (2011) 1–8

Contents lists available at SciVerse ScienceDirect

Journal of Catalysis

journal homepage: www.elsevier.com/locate/jcat

Mechanistic study of hydrocarbon formation in photocatalytic CO_2 reduction over Ti-SBA-15

Chieh-Chao Yang [a], Jarian Vernimmen [b], Vera Meynen [b], Pegie Cool [b], Guido Mul [a,*]

[a] PhotoCatalytic Synthesis Group, Faculty of Science and Technology, University of Twente, P.O. Box 217, 7500 AE Enschede, The Netherlands
[b] Laboratory of Adsorption and Catalysis, University of Antwerp, Universiteitsplein 1, B-2610 Wilrijk, Belgium

ARTICLE INFO

Article history:
Received 30 May 2011
Revised 5 August 2011
Accepted 5 August 2011
Available online 29 September 2011

Keywords:
CO_2 reduction
Photocatalysis
Ti-SBA-15
Solar fuels

ABSTRACT

Ti-SBA-15 was exposed to illumination in the presence of different gas mixtures containing CO or CO_2, and H_2O or H_2, in order to clarify the route to hydrocarbon formation in photocatalytic CO_2 reduction over this photocatalyst. A mixture of CO and H_2O led to the highest quantities of CH_4, C_2H_4, and C_2H_6 after 7 h of reaction, whereas a mixture of CO_2 and H_2 lead to the lowest production rate of these products. H_2O has been identified as more efficient in activation of CO and CO_2 than H_2. CH_3OH was not detected as significant product, and when fed to the catalyst, did not yield extensive product formation. Formaldehyde was found very reactive over the catalytic system, yielding a product distribution (C_1–C_2) of similar nature as obtained by CO activation. Finally, backward reactions, i.e., oxidation of hydrocarbon products into CO or CO_2, were found significant. Based on the experimental activity profiles, results indicated above, and available literature, a mechanism for photocatalytic CO_2 reduction is proposed involving the formation of CO in the initial stages, followed by consecutive formation of formaldehyde, which converts to CH_4, C_2H_4, and C_2H_6, presumably by reaction with photo-activated H_2O (OH radicals).

1. Introduction

Photocatalytic conversion of H_2O and CO_2 to fuel-like molecules is an ideal reaction to store solar energy in the form of chemical energy and to close the carbon cycle. However, there are several challenges to make this technology a reality. Predominantly, a poor conversion over various catalytic materials hinders practical application. TiO_2 was the first catalyst to be reported active in liquid-phase photocatalytic CO_2 reduction by Inoue et al. in 1979 [1]. Later in 1987, ruthenium loaded TiO_2 was found active in gas-phase photocatalytic CO_2 reduction, as reported by Thampi et al. [2]. Isolated Ti-sites in micro- and mesoporous materials were found very effective in CO_2 reduction by Yamashita et al. in 1995, including Ti-ZSM-5 [3]. Hwang et al. showed Ti-SBA-15 increased the CH_4 yield by two orders of magnitude when compared to TiO_2, and the CH_3OH yield by one order of magnitude in terms of μmol produced per gram Ti per hour [4]. In recent years, other materials effective in CO_2 reduction have been reported, such as Ti-nanotubes [5], metal loaded TiO_2 [6–10], and different novel types of semiconductors – like Ga_2O_3 [11], $InTaO_4$ [12,13], Zn_2GeO_4 [14], $Zn_2Ga_2O_4$ [15], and CdSe [16].

Among the above identified and investigated catalysts, those based on isolated titania in porous silica materials still hold the best reported performance upon UV exposure. Tetrahedrally coordinated Ti-sites are considered to be the active centers for catalyzing CO_2 into hydrocarbons [3,4]. However, various aspects of the catalysis are still unresolved. Anpo and coworkers have proposed a mechanism involving dissociation of CO_2 into CO and C, and H_2O into H and OH radicals, followed by recombination of the radicals to CH_4 and CH_3OH, with traces of C_2-products, and the co-product O_2 [17]. In a recent advanced IR study on Ti supported on MCM-41, however, only CO could be demonstrated as the product of reaction, and only if H_2O was co-fed to the IR cell [18]. The excitation of the Ti–O ligand-to-metal charge transfer was proposed to lead to transient Ti^{+III} and a hole on the framework oxygen. Electron transfer from Ti^{+III} to CO_2 splits the molecule into CO and O^-. O^- is spontaneously protonated by a Si–OH group or H^+ co-generated upon H_2O oxidation, to yield a surface adsorbed OH radical. The OH radicals either combine to yield H_2O_2 or dismutate to give O_2 and H_2O [18] .

Further understanding of the mechanism of UV-light-induced reduction in CO_2 by H_2O in Ti silicate sieves can lead to design rules for improved systems. Of particular interest is the identification of the individual reaction steps leading to the final products. Moreover, possible destructive reactions of final products need to be identified, since they will limit the quantum efficiency. In this article, the performance of Ti-SBA-15 is further evaluated. To better understand how isolated Ti-sites interact with potential intermediates, various gas mixtures including CO or CO_2, and H_2O or H_2 were used in illumination tests. By using standard C_1–C_3 gas mixtures, or pre-treatment in formic acid, methanol or formaldehyde, the

* Corresponding author.
E-mail address: G.Mul@utwente.nl (G. Mul).

0021-9517/$ - see front matter © 2011 Elsevier Inc. All rights reserved.
doi:10.1016/j.jcat.2011.08.005

backward reactions of hydrocarbons into CO or CO_2 were also investigated. The results will be discussed on the basis of potential mechanistic steps.

2. Experimental

2.1. Catalysts preparation

Ti-SBA-15 was synthesized by dissolving the surfactant, 4 g pluronic P123 ($EO_{20}PO_{70}EO_{20}$), in 20 mL $HCl_{(aq)}$ and 130 mL water. After mixing overnight, 9.14 mL TEOS (tetraethylorthosilicate) and 300 μL TBOT (titanium (IV) butoxide) were added under vigorous stirring, which was maintained for 7.5 h at 45 °C. The solution was aged overnight at 80 °C in an oil bath. After filtration, washing, drying, and calcination at 550°C for 6 h (1 °C/min) in air, Ti-SBA-15 was obtained. Pure SBA-15 was also prepared following a similar synthesis procedure, but without the addition of TBOT.

2.2. Catalytic evaluation

Gas-phase photocatalytic tests were performed in a custom-built combinatorial photoreactor system. The apparatus consists of three parts: the assembly of multiple batch photoreactors, a compact gas chromatograph, and a valve system controlled by a user interface in LabView. The 12 cylindrical reactors (inner volume 50 mL) are connected by a loop for gas dosage and sampling. To avoid cross-talk among reactors and disturbance from air, a diaphragm pump is used to evacuate the reactors and sampling loop down to 3 mbar. Fast quantitative analysis is achieved by a compact gas chromatograph, equipped with TCD and FID detectors. A combination of a Molsieve 5A column (5 m) and a capillary Porabond Q column (10 min) is connected to a TCD detector and used for the separation of H_2, O_2, N_2, CO, and CH_4. A Porabond Q column (10 m) is coupled to the FID detector, used for the separation and detection of C_1–C_4 alkanes and alkenes. Due to the short column length, and absence of a ramping procedure, quantitative data representing each reactor can be obtained within 80 s. The applied light source is a 120 W high-pressure mercury lamp. The spectrum of this mercury lamp ranges from 280 to 650 nm. A bundle of 12 quartz light guides is used to introduce the light source into the 12 reactors, in a homogeneous irradiance profile. The overall light irradiance (from 280 to 650 nm) reaching the bottom of each reactor is 1.5×10^5 μW/cm^2.

The production of hydrocarbons was monitored while Ti-SBA-15 was illuminated in the presence of various gas compositions of CO or CO_2, and H_2 or water vapor. By mixing a CO_2/He or CO/He stream with a H_2/He stream or He stream saturated with water vapor, these different initial gas compositions were obtained. Helium was used to maintain the overall pressure at 1.03 bar. Fifty milligrams of Ti-SBA-15 was used for testing in the target reactions. The catalyst samples were spread flatly at the bottom surface (35 mm in diameter) of the reactor. All the samples were pre-treated by illumination for 7 h in static humid Helium containing ca. 4 mol.% of water vapor (saturated at room temperature) to remove possible hydrocarbon contaminants. The effectiveness and details of contaminant removal will be addressed in the description of the results. After pre-illumination, three evacuation-gas dosage cycles were completed using evacuation of the reactor down to 3 mbar. Thus, the CO_2/He stream saturated with water vapor was introduced. All the reactors were operated in the batch mode and illuminated for 7 h. Production of hydrocarbons was quantified by the FID detector of the GC. The reaction was conducted with a ratio 0.5 of CO_2 (or CO) to H_2O (or H_2), containing 38 μmol of CO_2 (or CO) and 76 μmol of H_2O (or H_2). The temperature was maintained at 40 °C (±2 °C) during the 7 h of illumination. After each run of catalyst testing, the leftover gas reactants and products were removed by evacuation to 3 mbar. Three evacuation-gas dosage cycles were applied. The standard deviation in methane production was less than 0.5 ppm for all tests.

Additional experiments for the evaluation of potential backreactions of intermediates and products were conducted as follows: CH_4, C_2H_2, C_2H_4, C_2H_6, C_3H_4, C_3H_6, and C_3H_8 were used as initial reactants by the introduction of a standard gas mixture (Scotty analyzed gases, 15 ppm of each component in balance of nitrogen, 4 L, 120 psig, 21 °C) into a Helium stream saturated with or without water vapor (4 mol.% water vapor). For liquid reagents, the following procedure was applied: an amount of 50 mg of Ti-SBA-15 was dried at 120 °C overnight. The sample was then suspended in 10 mL of 99.9% CH_3OH (Sigma–Aldrich), 98% HCOOH (Merck), or 36.5% $HCHO_{(aq)}$ (Riedel – de Haën) (used as received) for 30 min. After filtration, the thus 'infused' samples were collected and directly used in illumination tests without drying.

2.3. Catalyst characterization

2.3.1. Textural properties

N_2 adsorption–desorption isotherms were obtained at liquid Nitrogen temperature using a Quantachrome Quadrasorb-SI automated gas adsorption system. Prior to an experiment, the sample was degassed at 200 °C for 16 h. The Brunauer–Emmet–Teller (BET) method was applied in a relative pressure range from 0.05 to 0.30 to calculate the specific surface area. The pore size distributions were deduced from the desorption branches of the isotherms using the Barrett–Joyner–Halenda (BJH) method. The total pore volumes were calculated from the amount of N_2 vapor adsorbed at a relative pressure of 0.95. ICP (Inductively Coupled Plasma) and EPMA (Electron Probe Micro Analysis) were applied for the elemental analysis. ICP was performed by using a PerkinElmer Optima 3000 dV apparatus. The EPMA analyses were performed on a JEOL JXA 733 apparatus to determine the Ti-loading of the Ti-SBA-15 sample.

2.3.2. In situ Diffuse Reflectance Infrared Fourier Transform Spectroscopy (DRIFTS)

In situ DRIFTS experiments were carried out using a Nicolet Magna 860 spectrometer equipped with a liquid N_2 cooled MCT detector, and a three window DRIFTS (Diffuse and Reflectance Infrared Fourier Transform Spectroscopy) cell. Two ZnSe windows allowed IR transmission, and a third (Quartz) window allowed the introduction of UV/Vis light into the cell. CO_2 (Linde Gas, 99.995%) was used as received. Prior to illumination, SBA-15 or Ti-SBA-15 was heated up to 120 °C in the cell and maintained at this temperature for 60 min, followed by cooling down to 30 °C in a dry He stream of 30 mL/min in order to remove physisorbed water. During illumination, the cell was kept at room temperature (30 °C). In situ IR spectra were recorded under UV/Vis light irradiation (100 W mercury lamp, λ: 250–600 nm), in the presence of a Helium atmosphere, against a background of the pre-treated catalyst. For comparison, other spectra were recorded accordingly against background spectra of the corresponding pre-treated samples, after saturation of the surface by exposure for 20 min to 4 mol.% water vapor in He or CO_2.

3. Results

3.1. Pre-illumination of Ti-SBA-15 in moist Helium

In a previous study, the contribution of carbon residue to CO production was demonstrated for Cu(I)/TiO_2, which can be greatly reduced by prolonged illumination in moist air [19]. Hence, in

order to minimize the influence of any possible carbon residue, the Ti-SBA-15 samples were all illuminated during 7 h in humid Helium conditions prior to the evaluation in photocatalytic reactions. Fig. 1a shows the formation of 3.5 ppm of CH_4, 1.4 ppm of C_2H_4, and 2.3 ppm of C_2H_6 as a result of illumination in humid Helium (1st illumination). Apparently, reactions of carbon residue yield the observed products, which even after calcination at 550°C for 6 h (1 °C/min) are still present in Ti-SBA-15. As shown in Fig. 1b and c, the production of CH_4, C_2H_4, and C_2H_6 largely decreased in subsequent illumination experiments in humid Helium and reached values of the same order as measured in an empty reactor as shown in Fig. 1d. All data reported in the remainder of this study were obtained after application of pre-illumination in humid Helium environment.

3.2. Illumination of Ti-SBA-15 in various gas mixtures

To investigate possible pathways to hydrocarbon formation over Ti-SBA-15, CH_4 and C_2-product formation in various mixtures of CO_2 or CO, and H_2O or H_2 was evaluated during illumination. As Fig. 2 demonstrates, CH_4, C_2H_4, and C_2H_6 are the primary products of CO_2 or CO activation. The highest yield was found for a mixture of CO and H_2O, i.e., 4.3 ppm CH_4, 2.5 ppm C_2H_4, and 3.7 ppm C_2H_6. Lower yields were obtained for a CO and H_2 mixture, and CO_2 and H_2O mixture, respectively, while the lowest yield was obtained for a CO_2 and H_2 mixture, i.e., 2.1 ppm CH_4, 1.4 ppm C_2H_4, and 0.8 ppm C_2H_6. The absence of CH_4 formation in the initial 3 h may be the result of the detection limit of the FID detector, being approximately 0.5 ppm. We therefore assume a relatively constant rate in CH_4 production in all conditions.

Taking the most productive condition (in the mixture of CO and H_2O) as an example, the amount of 4.3 ppm CH_4, 2.5 ppm C_2H_4, and 3.7 ppm C_2H_6 produced in the present study can be calculated to be the equivalent of 0.009 μmol CH_4, 0.005 μmol C_2H_4, and 0.007 μmol C_2H_6 after 7 h of illumination. The production rates of CH_4, C_2H_4, and C_2H_6 are thus 0.001, 0.0007, and 0.001 μmol/h, respectively. Considering that 0.05 g of Ti-SBA-15 catalysts was used, the yield of CH_4, C_2H_4, and C_2H_6 equals to 0.025, 0.014, and

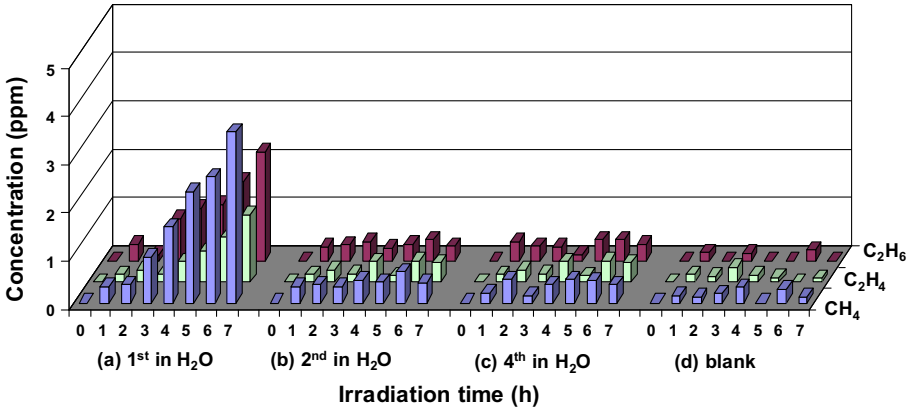

concentration (ppm)	(a) 1st in H_2O	(b) 2nd in H_2O	(c) 4th in H_2O	(d) blank
CH_4	3.54	0.47	0.37	0.12
C_2H_4	1.40	0.40	0.40	0.07
C_2H_6	2.26	0.31	0.35	-

Fig. 1. CH_4, C_2H_4, and C_2H_6 production over Ti-SBA-15 during 7 h of illumination in water vapor/Helium environment: (a) 1st illumination, (b) 2nd illumination, (c) 4th illumination, and (d) blank test. In-between illumination periods, the reactor was evacuated to 3 mbar, before reloading with humid He. The table shows the respective concentrations after 7 h of illumination.

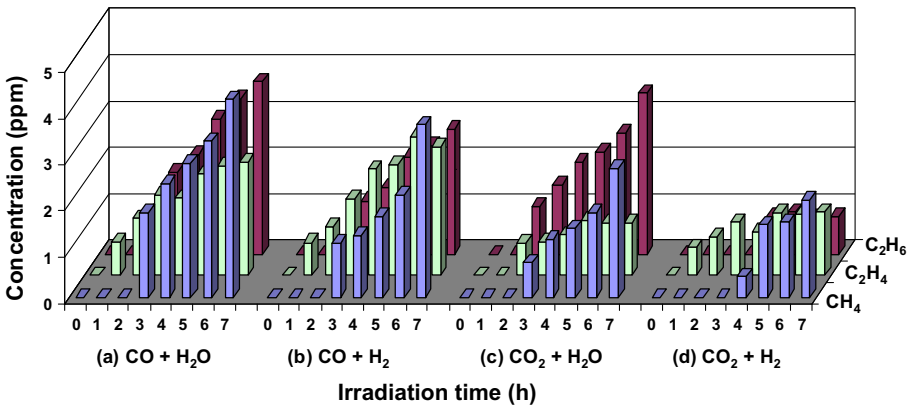

production (ppm)	(a) $CO + H_2O$	(b) $CO + H_2$	(c) $CO_2 + H_2O$	(d) $CO_2 + H_2$
CH_4	4.28	3.74	2.78	2.11
C_2H_4	2.46	2.79	1.15	1.39
C_2H_6	3.74	2.71	3.50	0.81

Fig. 2. CH_4, C_2H_4, and C_2H_6 production over Ti-SBA-15 during 7 h of illumination in various gas mixtures: (a) $CO/H_2O = 0.5$, (b) $CO/H_2 = 0.5$, (c) $CO_2/H_2O = 0.5$, and (d) $CO_2/H_2 = 0.5$. The table shows the respective concentrations after 7 h of illumination.

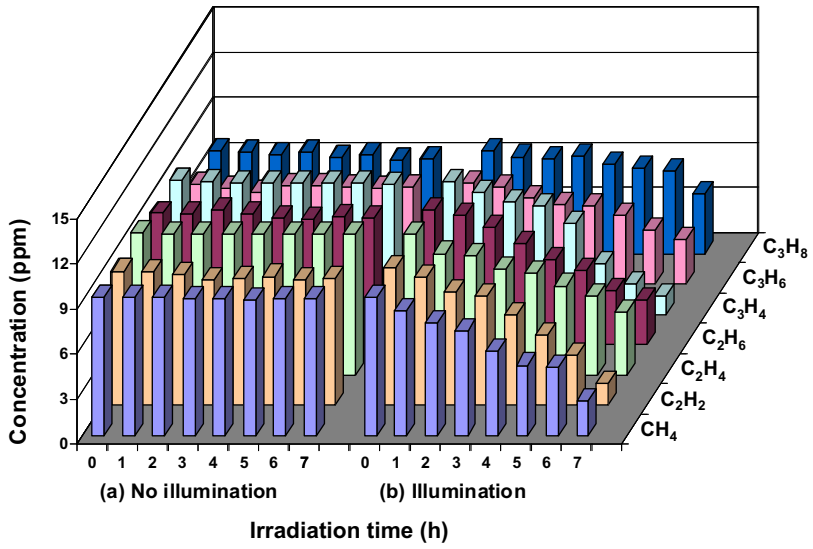

condition		concentration (ppm)						
		CH_4	C_2H_2	C_2H_4	C_2H_6	C_3H_4	C_3H_6	C_3H_8
(a) no illumination	0th h	9.22	8.92	9.44	8.73	8.89	6.63	6.85
	7th h	9.08	8.44	9.38	8.40	8.63	6.45	6.35
(b) illumination	0th h	9.16	9.17	9.39	8.99	8.84	6.73	6.86
	7th h	2.29	1.42	4.14	2.92	1.24	2.97	4.00

Fig. 3. Concentrations of C1–C3 alkanes, alkenes, and alkynes in the presence of Ti-SBA-15: (a) no illumination and (b) illumination for 7 h. The initial concentrations are 9 ppm CH_4, C_2H_2, C_2H_4, C_2H_6, C_3H_4, and 7 ppm C_3H_6, C_3H_8, respectively. Total pressure: 1.03 bar Helium. The table shows the respective concentrations after 7 h of illumination.

0.021 μmol/g-cat/h. Based on the elemental analysis (ICP) of the Ti-loading in Ti-SBA-15 (0.05 wt%), the yields of CH_4, C_2H_4, and C_2H_6 are 49.75, 28.93, and 42.81 μmol/g-Ti/h. Assuming that all the Ti-sites were accessible for the reaction, the turnover frequency of CH_4, C_2H_4, and C_2H_6 can also be calculated as 2.4×10^{-3}, 1.4×10^{-3}, and 2.0×10^{-3} h^{-1}. In this regard, after 7 h of reaction time, roughly only 1 out of 1000 Ti-sites has been active in producing CH_4, C_2H_4, and C_2H_6 by conversion of CO and H_2O.

3.3. Backward reaction, C_1–C_3 hydrocarbons into CO_2

Ti-SBA-15, pre-illuminated in humid Helium, was illuminated in a gas mixture of CH_4, C_2H_2, C_2H_4, C_2H_6, C_3H_4, C_3H_6, and C_3H_8 to analyze the rate of oxidation of these hydrocarbons. Fig. 3a demonstrates the absence of concentration changes in various components in the dark. During 7 h of illumination, Fig. 3b, the concentration of all C_1–C_3 alkanes, alkenes, and alkynes decreased. CH_4 decreased from 9.2 ppm to 2.3 ppm. The other C_2 and C_3 compounds also decreased in concentration with conversion levels higher than 50%. Physisorbed water on the catalyst and traces of oxygen left in the reactor after evacuation probably initiated the conversion of the C_1–C_3 compounds into CO or CO_2. Summarizing, the backward reaction – hydrocarbon oxidation to CO or CO_2 – is feasible during illumination.

3.4. Oxygenates?

Contrary to the sole production of alkanes and alkenes (mainly CH_4) observed in the present study, CH_3OH was found as primary product in the literature over Ti-ZSM-5 [3], Ti-MCM-41, Ti-MCM-48 [20], Ti-FSM-16 [21], Ti-Beta zeolites [22], Ti-containing nanoporous silica films [23], and Ti-SBA-15 [4]. To further clarify whether and how CH_3OH or other oxygenates are involved in CO_2 reduction, CH_3OH, HCHO, and HCOOH-infused Ti-SBA-15 samples were prepared and exposed to illumination. As shown in Fig. 4a, 1.3 ppm CH_4, 0.9 ppm C_2H_4, and 0.9 ppm C_2H_6 was detected for the CH_3OH-infused Ti-SBA-15 sample after 7 h of illumination in Helium. 1.9 ppm CH_4, 0.8 ppm C_2H_4, and 0.9 ppm C_2H_6 was found to be formed after illuminating a HCOOH-infused Ti-SBA-15 sample for 7 h. Compared with illumination of Ti-SBA-15 in CO_2 and water vapor (Fig. 4d), the improvement in CH_4, C_2H_4, and C_2H_6 production was not significant for the CH_3OH- and HCOOH-infused samples. On the contrary, for the HCHO-infused Ti-SBA-15 sample, a huge amount of CH_4 and C_2H_6 was produced (inset in Fig. 4). As much as 436 ppm of CH_4 and 19.4 ppm of C_2H_6 were produced after 7 h of illumination. Surprisingly, C_2H_4 was detected in only very little amounts. This observation implies that formaldehyde is extremely reactive over Ti-SBA-15, although direct photolysis reactions are also contributing to conversion, as will be discussed later.

3.5. Catalyst stability

It has been demonstrated in the literature that the meso-structure of SBA-15 will largely collapse as a result of steam treatment at temperatures higher than 600 °C [24,25]. Hydrolysis and dehydrolysis can cause the recombination of Si–O–Si bonds on the amorphous silica walls of SBA-15, especially where numerous silanol groups are located. Although the working temperature and conditions of photocatalytic CO_2 reduction with water vapor are not as severe as steam at elevated temperatures, it is essential to evaluate whether the pore structure remains intact during illumination. Fig. 5 shows N_2 adsorption–desorption isotherms and the pore size distribution (based on the desorption curve) of Ti-SBA-15. The characteristic feature of a Type IV isotherm with hysteresis loop is evident, which is associated with capillary condensation in

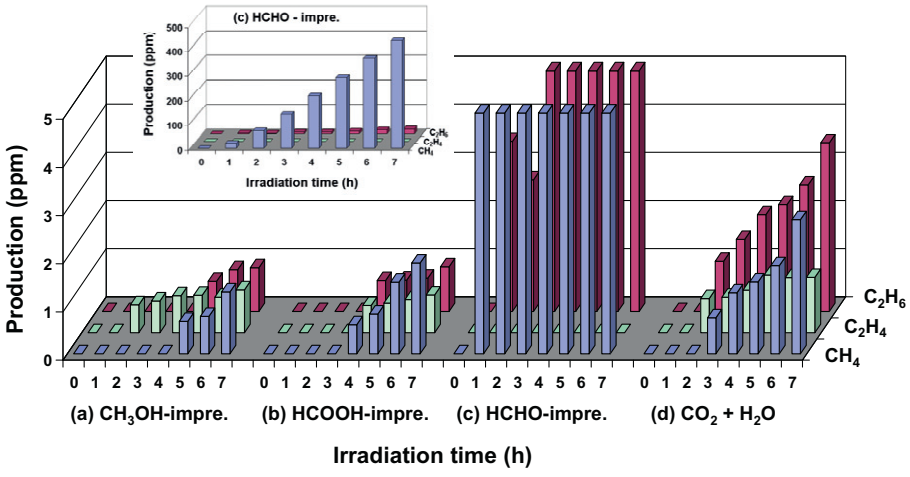

production (ppm)	(a) CH_3OH-impre.	(b) HCOOH-impre.	(c) HCHO-impre.	(d) $CO_2 + H_2O$
CH_4	1.28	1.88	436.05	2. 78
C_2H_4	0.89	0.78	-	1.15
C_2H_6	0.91	0.93	19.38	3.50

Fig. 4. CH_4, C_2H_4, and C_2H_6 production over Ti-SBA-15 infused with (a) CH_3OH, (b) HCOOH, and (c) HCHO during 7 h of illumination in Helium environment, compared with Ti-SBA-15 illuminated in (d) CO_2/H_2O. The table shows the respective concentrations after 7 h of illumination.

mesopores [26]. Based on the isotherm in Fig. 5a and the pore size distributions in Fig. 5b, the pore structure was established to be stable during illumination in the presence of CO_2 and H_2O. Table 1 indicates a slight decrease in BET surface (from 852 to 816 cm^2/g) and pore volume (from 0.96 to 0.93 cm^3/g), comparing fresh Ti-SBA-15 and Ti-SBA-15 illuminated in the presence of CO_2/H_2O. The isotherm of SBA-15 shows the same hysteresis profile as Ti-SBA-15, in agreement with the low Ti-loading of the used Ti-SBA-15 catalyst (0.05 wt% from ICP and 0.1 wt% from EPMA).

Fig. 6 shows the DRIFT spectra of Ti-SBA-15 and SBA-15 in specific working conditions, recorded against the spectra of the respective dehydrated samples. As shown in Fig. 6a, in addition to the signature of the broad band in the region of 2800 and 3800 cm^{-1} assigned to chemisorbed water and H-bonded OH groups, spectral enhancement is visible at 910 and 950 cm^{-1}, and depletion at 3744 cm^{-1}, when exposing Ti-SBA-15 to water vapor for 20 min. A similar spectral signature, Fig. 6b, was observed for SBA-15, except for the absorption at 910 cm^{-1}. The 910 cm^{-1} absorption has been assigned to the vibration of Si–O–Ti bonds [27], while the 950 cm^{-1} band is assigned to dangling $\nu(Si–O_d)$ vibrations associated with Si–OH and $Si–O^-$ groups [28–30]. The 3744 cm^{-1} band is the corresponding OH stretching vibration of isolated surface silanol groups [31]. After 7 h of illumination in the presence of water vapor, the 910 and 950 cm^{-1} bands increased, while a further depletion at 3744 cm^{-1} was observed for Ti-SBA-15. The spectra of SBA-15 remained practically unchanged during illumination.

In the case of exposing Ti-SBA-15 or SBA-15 to CO_2 and water vapor, similar spectral profiles were observed. The only difference is the presence of two doublet absorption bands at 3600–3630 and 3715–3740 cm^{-1}, which are assigned to gas-phase CO_2 [32]. The depletion of silanol groups at 3744 cm^{-1} needs to be considered when CO_2 and water vapor are introduced. The enhancement of the CO_2 doublet around 3715–3740 cm^{-1} overlaps with the depletion of silanol groups at 3744 cm^{-1}, resulting in various negative features around 3715–3740 cm^{-1}. Upon illumination, irrespective of the present gas mixture (water vapor in the absence or presence of CO_2) for Ti-SBA-15, the 910 and 950 cm^{-1} absorption bands increased, while the band at 3744 cm^{-1} decreased. In contrast, these bands remained identical for SBA-15 in all conditions.

4. Discussion

4.1. CO_2 reduction over Ti-SBA-15: mechanistic considerations

First, it is important to mention that carbon residues might contribute to product formation in CO_2 reduction in the presence of H_2O. This is clearly demonstrated by the data reported in Fig. 1. Carbon-containing reagents are often used in Ti-catalyst synthesis, such as for Ti-nanotube materials [5], as well as the SBA-15 catalysts reported herein. It is difficult to establish the nature of the carbon residues left after material synthesis [21]. It is clear, however, that illumination pre-treatment of the catalyst in the presence of water is a more efficient way to remove carbon residue than calcination in air at elevated temperatures.

Fig. 2 clearly demonstrates that CO_2 reduction is feasible in the presence of H_2O, to yield CH_4 and C_2 products. It is proposed that CO is an important intermediate in the conversion of CO_2 to CH_4. This is in agreement with various observations. First, conversion of CO_2 to CH_4 was also reported by Saladin et al. over Degussa P25 TiO_2 catalyst [33], and CO demonstrated an intermediate in the production of CH_4. Also, in situ IR studies [19], indicate CO formation to be quite feasible by photo-activation of CO_2 in the presence of a $Cu(I)/TiO_2$ catalyst. Second, Fig. 2 demonstrates CO is quite reactive to form a similar product distribution as observed by the activation of CO_2. The reason CO was not observed in these experiments is likely that the rate of formation of CO by CO_2 activation is apparently slower than the rate of conversion of CO to CH_4.

Comparing Fig. 2c and d shows that H_2O is more efficient than H_2 to reduce CO_2 into CH_4 over Ti-SBA-15. Considering the bond energy of the H–H bond (436 kJ/mol, at 25 °C), which is slightly lower than of the O–H bond in water (464 kJ/mol, at 25 °C) [34], this appears remarkable. However, the interaction between H_2 or H_2O and the "active sites" on the materials and the necessity of an electron donor (water oxidation with formation of O_2) also need to be considered. Fig. 6a shows the increase in the dangling bond $\nu(Si–O_d)$ and decrease in surface silanol groups, respectively, when exposing Ti-SBA-15 to water vapor. These spectral observations indicate strong interaction between H_2O and Ti-SBA-15 [30].

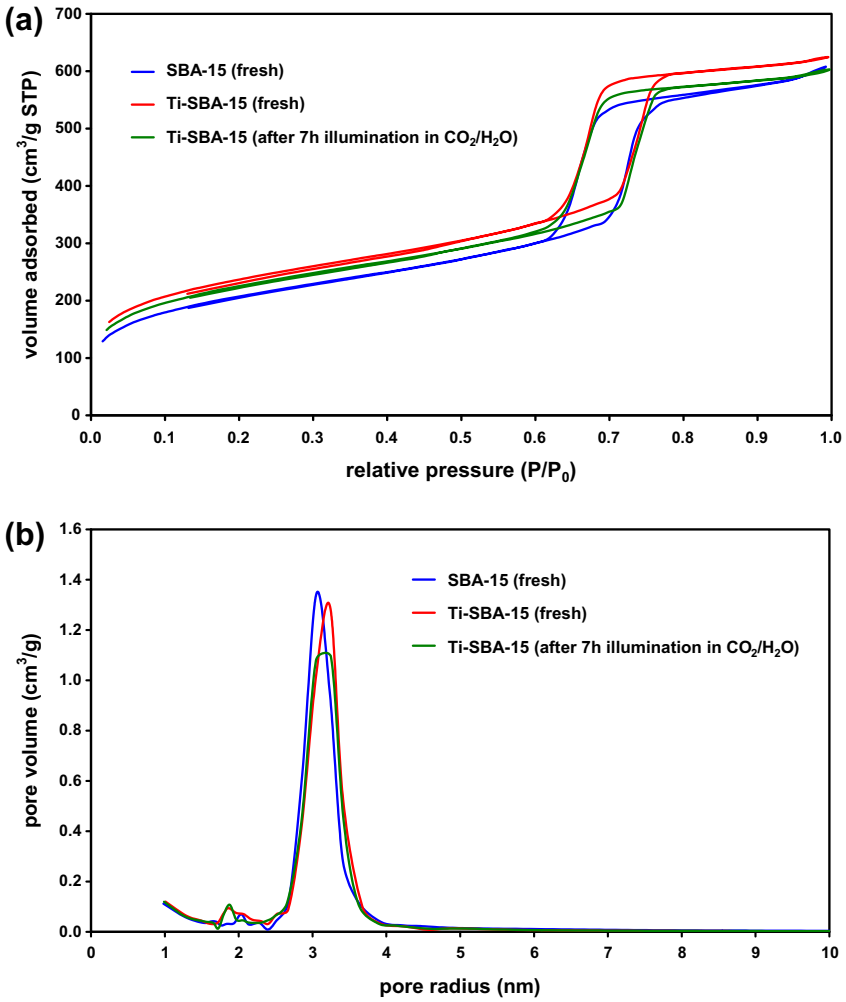

Fig. 5. (a) Isotherm of N_2 adsorption and (b) desorption pore size distribution of the SBA-15 and Ti-SBA-15 samples: fresh, and after 7 h of illumination in CO_2/H_2O. (For interpretation of the references to color in this figure legend, the reader is referred to the web version of this article.)

Table 1
Textural properties of SBA-15 and Ti-SBA-15.

	BET surface area (m^2/g)	Total pore volume (cm^3/g)	Average pore radius[a] (nm)
SBA-15	751	0.93	3.1
Ti-SBA-15	852	0.96	3.2
Ti-SBA-15 illum. in CO_2/H_2O	816	0.93	3.2

[a] The average pore radius was determined by the desorption isotherm of the investigated samples.

4.2. Role of oxygenates?

In literature reports, CH_3OH was found to be one of the primary products in gas-phase CO_2 reduction over isolated titania on porous materials [3,4,20–23]. However, in this study, CH_3OH was not detected in the illumination tests of various gas compositions, as shown in Fig. 2. Moreover, the IR spectra of Ti-SBA-15 while illuminated in the presence of CO_2 and H_2O showed no signature of adsorbed CH_3OH or other absorption bands indicative of adsorbed oxygenates (e.g., formates or aldehydes). As Fig. 6 demonstrates, absorptions related to methyl stretching vibrations in the region between 2600 and 3000 cm^{-1} are absent, in agreement with the absence of CH_3OH production over Ti-SBA-15. Fig. 4 shows conversion of CH_3OH into C_1–C_2 hydrocarbons occurs only to a limited extent, which makes methanol an unlikely intermediate in the conversion of CO_2 to methane. The observed (slow) conversion of CH_3OH might be related to primary decomposition into CO or CO_2, and consecutive reaction of CO or CO_2 into hydrocarbons. Pre-treatment of Ti-SBA-15 by HCOOH-impregnation resulted in even lower production of C1–C2 hydrocarbons than after CH_3OH-infusion, which excludes HCOOH as significant intermediate in CO_2 reduction. However, a dramatic increase in CH_4 production was observed after HCHO addition to Ti-SBA-15.

4.3. Mechanism

Based on the above-discussed observations, we propose a tentative mechanism of CO_2 reduction by H_2O over Ti-SBA-15, as shown in Fig. 7. We follow the proposed route by Frei et al. to explain formation of CO. In this route, a Ti–OH site serves as the active site for the adsorption of CO_2 and H_2O. The photo-induced $[Ti(III)–O(I)]^*$ site delivers electrons to CO_2, splitting this into CO [18]. The first light-induced reaction in the scheme of Fig. 7 comprises the overall reaction of the intermediate steps proposed by Frei and coworkers, with the assumption that the formation of hydrogen peroxide (the result of recombination of two OH-radicals) in turn leads to a hydroperoxo – Ti–OOH – intermediate [18,35,36]. Nakamura et al. reported spectroscopic evidence of the light-induced

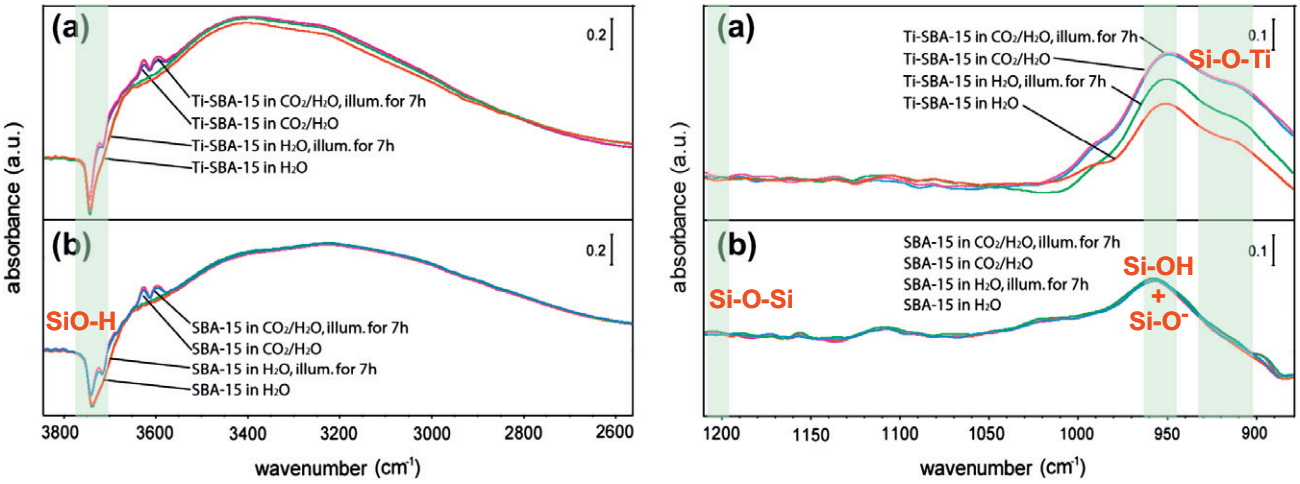

Fig. 6. DRIFT spectra of (a) Ti-SBA-15 and (b) SBA-15, under various conditions: (1) after dosing H_2O/He for 20 min, (2) after illumination in H_2O/He for 7 h, (3) after dosing CO_2/H_2O for 20 min, and (4) after illumination in CO_2/H_2O for 7 h. All the spectra were recorded against the spectra of the respective dehydrated samples after heat treatment at 120 °C.

formation of such Ti–OOH hydroperoxo species on nanocrystalline TiO_2 films in contact with aqueous solution, all be it in the presence of O_2 [35]. Due to the limited amount and short lifetime, Ti–OOH was not successfully detected by IR spectroscopy in the present study. For completeness, we included the water-mediated formation of the hydroperoxide species in Fig. 7, presumably as a minor contributor, since H_2 was not observed experimentally in the present study.

Besides decomposition of the peroxide to oxygen [36], we propose a subsequent reaction of the peroxide with CO and H_2O to form HCHO, in which the hydroperoxo species is converted to Ti–OH by releasing one molecule of O_2. Based on the very high rate of CH_4 formation by the HCHO-pre-treated Ti-SBA-15 system observed in Fig. 4, the conversion of HCHO to CH_4 occurs effectively and fast by reaction with photo-activated H_2O, another molecule of O_2 being produced consequently. Unfortunately, the generation of O_2 was not demonstrated experimentally, probably because this is consumed by consecutive reactions.

C_2H_4 and C_2H_6 are potential products of the reaction of two molecules of HCHO, in the presence or absence of H_2O, respectively. As shown in Fig. 4, illumination of HCHO-infused Ti-SBA-15 yields CH_4 and C_2H_6, while C_2H_4 is barely formed. This suggests a significant quantity of water was still present in Ti-SBA-15 during this experiment, which is very likely given the followed procedure of pre-treating Ti-SBA-15 with HCHO. It should be mentioned that the extremely high conversion of formaldehyde to hydrocarbons is remarkable. In the literature, the photodecomposition of

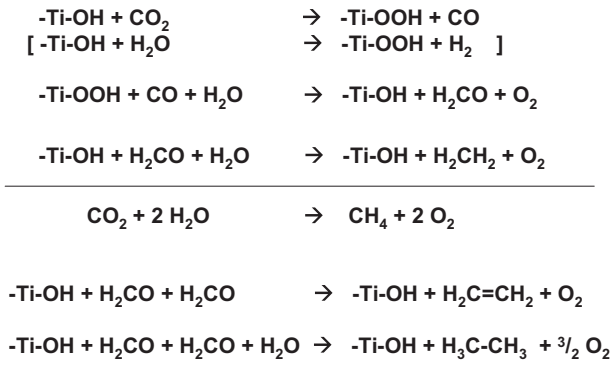

Fig. 7. Proposed mechanism of photocatalytic CO_2 reduction with H_2O over Ti-SBA-15.

formaldehyde has been studied by mixing different quantities of formaldehyde in synthetic air [37]. CO and H_2 were found to be the major products upon illumination in the wavelength range of 290–330 nm. Pope and his coworkers have recently discussed the photochemistry in more detail. Besides the photon-induced splitting of formaldehyde into CO and H_2, also other reactions have been proposed, in particular between OH-radicals and formaldehyde, leading to HCO and H_2O, or direct decomposition to HCO and H (below 330 nm). Subsequent oxidation of HCO by oxygen leads to HO_2 and CO. Photochemistry thus very likely significantly contributes to the observed product distribution in the formaldehyde experiment, including the formation and decomposition of peroxide intermediates [38]. However, the formation of CH_4 and C_2 products is not disclosed in these photochemistry studies, and potentially involves photocatalytic steps, as tentatively proposed in Fig. 7. The photocatalytic and simultaneous photochemical transformations of formaldehyde are numerous and need to be studied in more detail in the presence of the Ti-SBA-15 catalyst. In situ DRIFTS studies are planned, including the use of ^{13}C-labeled formaldehyde, to evaluate the formation of C–C bonds.

Furthermore, it should be mentioned that our mechanism is a rather 'global' description. Obviously, various additional intermediate steps (e.g., carbon formation from CO_2 decomposition and related molecules such as formaldehyde) might be involved, but we cannot evaluate these based on the data presented in the present study. We like to mention the ESR data reported by Anpo et al. [17], which appear to indicate the presence of various radical fragments on the surface of the catalyst formulation during illumination, again in agreement with various pathways proposed for the photochemical decomposition of formaldehyde.

4.4. Catalyst alterations for improving performance

A significant extent of oxidation of hydrocarbons into CO or CO_2 was observed in Fig. 3a and b. This is an important observation, which suggests that if oxygen produced in the reaction by water oxidation is not efficiently removed from the catalytic sites, this will inevitably lead to lower quantum efficiencies. Achieving this by, for example, pore structure optimization would be an important means to further improve performance of this intriguing photo-catalytically active system. At the same time, the oxidation potential of intermediates formed in the process of water oxidation is also significant, and these might contribute even more effectively to hydrocarbon oxidation. This would require physical

separation of oxidation and reduction sites, with various synthetic challenges.

Another way forward is to increase the number of "active sites" for CO_2 reduction. Trukhan et al. showed that a certain amount of Ti species might be embedded in the thick amorphous silica walls, with poor catalytic activity in oxidation reactions [39]. Extraction of these sites by, e.g., mild steam treatment might create a higher effective quantity of active sites. This might also improve the accessibility. An adverse effect might be the structural degradation of the catalysts and condensation of isolated sites to form TiO_2 nanocrystals after contact with water, which should be prevented [40].

Surface modification to enhance CO_2 adsorption may be another solution to boost the effectiveness of the catalytic sites. SBA-15 functionalization with Lewis bases (primary, secondary, and tertiary amines) was reported to increase the number of active sites for CO_2 activation, utilized in cyclic carbonate synthesis [41]. Future studies are needed to verify whether the above-mentioned structural changes will lead to improved performance.

5. Conclusions

In this study, a mechanism of CO_2 reduction over Ti-SBA-15 is presented, based on the reactivity of the catalyst in various initial gas mixtures of CO or CO_2, and H_2O or H_2. The results indicate that the highest rate of hydrocarbon production is achieved with a mixture of CO and H_2O. H_2 activation is not as efficient as H_2O activation, probably due to a poor interaction with isolated Ti sites. We believe in a mechanism for CO_2 reduction in which CO and formaldehyde are important intermediates, and in which transient Ti–OOH species are likely involved.

Acknowledgments

This work was supported by ACTS (NWO, The Netherlands), in the framework of an NSC-NWO project (Project No. NSC-97-2911-I-002-002). Ruben Lubkemann at University of Twente is gratefully acknowledged for technical support. Jarian Vernimmen thanks the Fund for Scientific Research – Flanders (FWO-Vlaanderen) for financial support.

References

[1] T. Inoue, A. Fujishima, S. Konishi, K. Honda, Nature 277 (1979) 637.
[2] K.R. Thampi, J. Kiwi, M. Gratzel, Nature 327 (1987) 506.
[3] H. Yamashita, A. Shiga, S. Kawasaki, Y. Ichihashi, S. Ehara, M. Anpo, Energy Convers. Manage. 36 (1995) 617.
[4] J.S. Hwang, J.S. Chang, S.E. Park, K. Ikeue, M. Anpo, Top. Catal. 35 (2005) 311.
[5] O.K. Varghese, M. Paulose, T.J. LaTempa, C.A. Grimes, Nano Lett. 9 (2009) 731.
[6] N. Sasirekha, S.J.S. Basha, K. Shanthi, Appl. Catal. B 62 (2006) 169.
[7] I.H. Tseng, J.C.S. Wu, H.Y. Chou, J. Catal. 221 (2004) 432.
[8] H.C. Yang, H.Y. Lin, Y.S. Chien, J.C.S. Wu, H.H. Wu, Catal. Lett. 131 (2009) 381.
[9] K. Koci, K. Mateju, L. Obalova, S. Krejcikova, Z. Lacny, D. Placha, L. Capek, A. Hospodkova, O. Solcova, Appl. Catal. B 96 (2010) 239.
[10] Q.H. Zhang, W.D. Han, Y.J. Hong, J.G. Yu, Catal. Today 148 (2009) 335.
[11] H. Tsuneoka, K. Teramura, T. Shishido, T. Tanaka, J. Phys. Chem. C 114 (2010) 8892.
[12] P.W. Pan, Y.W. Chen, Catal. Commun. 8 (2007) 1546.
[13] Z.Y. Wang, H.C. Chou, J.C.S. Wu, D.P. Tsai, G. Mul, Appl. Catal. A 380 (2010) 172.
[14] Q. Liu, Y. Zhou, J.H. Kou, X.Y. Chen, Z.P. Tian, J. Gao, S.C. Yan, Z.G. Zou, J. Am. Chem. Soc. 132 (2010) 14385.
[15] S.C. Yan, S.X. Ouyang, J. Gao, M. Yang, J.Y. Feng, X.X. Fan, L.J. Wan, Z.S. Li, J.H. Ye, Y. Zhou, Z.G. Zou, Angew. Chem. Int. Ed. 49 (2010) 6400.
[16] C.J. Wang, R.L. Thompson, J. Baltrus, C. Matranga, J. Phys. Chem. Lett. 1 (2010) 48.
[17] M. Anpo, H. Yamashita, Y. Ichihashi, S. Ehara, J. Electroanal. Chem. 396 (1995) 21.
[18] W.Y. Lin, H.X. Han, H. Frei, J. Phys. Chem. B 108 (2004) 18269.
[19] C.C. Yang, Y.H. Yu, B. van der Linden, J.C.S. Wu, G. Mul, J. Am. Chem. Soc. 132 (2010) 8398.
[20] H. Yamashita, Y. Fujii, Y. Ichihashi, S.G. Zhang, K. Ikeue, D.R. Park, K. Koyano, T. Tatsumi, M. Anpo, Catal. Today 45 (1998) 221.
[21] K. Ikeue, H. Mukai, H. Yamashita, S. Inagaki, M. Matsuoka, M. Anpo, J. Synchrotron Radiat. 8 (2001) 640.
[22] K. Ikeue, H. Yamashita, T. Takewaki, M.E. Davis, M. Anpo, J. Synchrotron Radiat. 8 (2001) 602.
[23] I. Keita, S. Nozaki, M. Ogawa, M. Anpo, Catal. Today 74 (2002) 241.
[24] K. Cassiers, T. Linssen, M. Mathieu, M. Benjelloun, K. Schrijnemakers, P. Van Der Voort, P. Cool, E.F. Vansant, Chem. Mater. 14 (2002) 2317.
[25] F.Q. Zhang, Y. Yan, H.F. Yang, Y. Meng, C.Z. Yu, B. Tu, D.Y. Zhao, J. Phys. Chem. B 109 (2005) 8723.
[26] K.S.W. Sing, D.H. Everett, R.A.W. Haul, L. Moscou, R.A. Pierotti, J. Rouquerol, T. Siemieniewska, Pure Appl. Chem. 57 (1985) 603.
[27] C. Beck, T. Mallat, T. Burgi, A. Baiker, J. Catal. 204 (2001) 428.
[28] J. Pires, M. Pinto, J. Estella, J.C. Echeverria, J. Colloid Interface Sci. 317 (2008) 206.
[29] A. Fidalgo, L.M. Ilharco, Chem. Eur. J. 10 (2004) 392.
[30] G. Ricchiardi, A. Damin, S. Bordiga, C. Lamberti, G. Spano, F. Rivetti, A. Zecchina, J. Am. Chem. Soc. 123 (2001) 11409.
[31] J.P. Gallas, J.C. Lavalley, A. Burneau, O. Barres, Langmuir 7 (1991) 1235.
[32] K.E. Dierenfeldt, J. Chem. Edu. 72 (1995) 281.
[33] F. Saladin, L. Forss, I. Kamber, J. Chem. Soc. Chem. Commun. (1995) 533.
[34] R.T. Sanderson, Chemical Bonds and Bond Energy, second ed., Academic Press, New York, 1976.
[35] R. Nakamura, A. Imanishi, K. Murakoshi, Y. Nakato, J. Am. Chem. Soc. 125 (2003) 7443.
[36] N. Ulagappan, H. Frei, J. Phys. Chem. A 104 (2000) 7834.
[37] G.K. Moortgat, P. Warneck, J. Chem. Phys. 70 (1979) 3639.
[38] F.D. Pope, C.A. Smith, P.R. Davis, D.E. Shallcross, M.N.R. Ashfold, A.J. Orr-Ewing, Faraday Discuss. 130 (2005) 59.
[39] N.N. Trukhan, V.N. Romannikov, A.N. Shmakov, M.P. Vanina, E.A. Paukshtis, V.I. Bukhtiyarov, V.V. Kriventsov, I.Y. Danilov, O.A. Kholdeeva, Micropor. Mesopor. Mater. 59 (2003) 73.
[40] M.J. Elser, T. Berger, D. Brandhuber, J. Bernardi, O. Diwald, E. Knozinger, J. Phys. Chem. B 110 (2006) 7605.
[41] R. Srivastava, D. Srinivas, P. Ratnasamy, Micropor. Mesopor. Mater. 90 (2006) 314.